BeF_3^- acts as a phosphate analog in proteins phosphorylated on aspartate: Structure of a BeF_3^- complex with phosphoserine phosphatase

Ho Cho*, Weiru Wang*, Rosalind Kim*, Hisao Yokota*, Steven Damo*, Sung-Hou Kim*†, David Wemmer*†‡, Sydney Kustu‡§, and Dalai Yan§¶

*Physical Biosciences Division, Lawrence Berkeley National Laboratory, 1 Cyclotron Road, Berkeley, CA 94720; and Departments of †Chemistry and §Plant and Microbial Biology, University of California, Berkeley, CA 94720

Contributed by Sydney Kustu, April 27, 2001

Protein phosphoaspartate bonds play a variety of roles. In response regulator proteins of two-component signal transduction systems, phosphorylation of an aspartate residue is coupled to a change from an inactive to an active conformation. In phosphatases and mutases of the haloacid dehalogenase (HAD) superfamily, phosphoaspartate serves as an intermediate in phosphotransfer reactions, and in P-type ATPases, also members of the HAD family, it serves in the conversion of chemical energy to ion gradients. In each case, lability of the phosphoaspartate linkage has hampered a detailed study of the phosphorylated form. For response regulators, this difficulty was recently overcome with a phosphate analog, BeF_3^-, which yields persistent complexes with the active site aspartate of their receiver domains. We now extend the application of this analog to a HAD superfamily member by solving at 1.5-Å resolution the x-ray crystal structure of the complex of BeF_3^- with phosphoserine phosphatase (PSP) from *Methanococcus jannaschii*. The structure is comparable to that of a phosphoenzyme intermediate: BeF_3^- is bound to Asp-11 with the tetrahedral geometry of a phosphoryl group, is coordinated to Mg^{2+}, and is bound to residues surrounding the active site that are conserved in the HAD superfamily. Comparison of the active sites of BeF_3^-·PSP and BeF_3^-·CeY, a receiver domain/response regulator, reveals striking similarities that provide insights into the function not only of PSP but also of P-type ATPases. Our results indicate that use of BeF_3^- for structural studies of proteins that form phosphoaspartate linkages will extend well beyond response regulators.

Protein phosphorylation plays critical roles in cellular control. Phosphorylation of aspartate residues is central to the function of two large protein families, response regulators and the haloacid dehalogenase (HAD) superfamily of hydrolases (1, 2).

Response regulators and their cognate histidine kinases constitute two-component systems (3), which dominate signal transduction in bacteria and are also present in archaea, microbial eukarya, and higher plants. Response regulators have in common a homologous regulatory module of ≈120-aa residues called a receiver domain. Receiver domains have an $(\alpha/\beta)_5$ fold and an active site defined by a quintet of highly conserved residues composed of three aspartates, a lysine, and either a threonine or a serine. Phosphorylation of the active site aspartate residue in a receiver domain is coupled to a conformational change that regulates the function of its output domain or downstream target protein. CheY, the central regulator of bacterial chemotaxis, is a well-studied response regulator. When phosphorylated, this single domain protein, which can also be described as a receiver domain, binds to the FliM protein in the basal body of the flagellum to reverse the direction of flagellar rotation (4, 5).

For many years, the lability of phosphoaspartate linkages in receiver domains limited structural studies to their unphosphorylated inactive forms. Recently, several structures of activated receiver domains were obtained by using a variety of means to overcome the problem of lability (6–10). Among these, formation of a complex with BeF_3^-, which yields an excellent aspartyl phosphate mimic, appears to be a simple general solution (11). BeF_3^- readily forms persistent activated complexes with many response regulators, regardless of the half-lives of their phosphorylated states.

Members of the HAD superfamily of hydrolases have diverse functions (12–14). Although 2-haloacid dehalogenase, the founding member of this large protein family, does not catalyze hydrolysis of phosphorylated substrates or depend on a divalent cation, most other members do. For example, the phosphotransferase subgroup includes several phosphatases, among them phosphoserine phosphatase (PSP), and some phosphomutases. The subgroup of P-type ATPases serves in transport of cations across biological membranes (15–17). Phosphoenzyme intermediates have been detected among the phosphotransferases of the HAD superfamily (14, 18–20) and are known to form during the catalytic cycle of P-type ATPases (1, 15–17). In both cases, phosphorylation requires a divalent cation, normally Mg^{2+}, and occurs at a conserved aspartate residue. In addition, there is biochemical evidence that vanadate binds to phosphatases and phosphomutases in the HAD superfamily (19, 21) and that vanadate, beryllofluoride, and aluminum fluoride, all of which can act as phosphate analogs, bind to P-type ATPases (22–28).

The core catalytic domains of HAD family phosphotransferases and P-type ATPases share the same quintet of highly conserved residues found in receiver domains (12, 29), although a circular permutation is required to align the primary sequences of members of these two large families (29). High-resolution crystal structures of HAD superfamily members [haloacid dehalogenases from *Pseudomonas* sp. YL and *Xanthobacter autotrophicus* GJ10 (30, 31), the Ca^{2+}-ATPase from rabbit sarcoplasmic reticulum (32), and PSP from *Methanococcus jannaschii* (33)] indicate that the catalytic domains of these proteins form a typical α/β Rossmann fold that is similar to that in CheY (29). The quintet of conserved residues noted above surrounds the active site, as it does in receiver domains. These commonalities led to proposals of a common reaction mechanism for the formation of the phosphoaspartate bond (12, 29). They also raise

BIOCHEMISTRY

Abbreviations: HAD, haloacid dehalogenase; PSP, phosphoserine phosphatase; FHSQC, fast heteronuclear single quantum correlation; P domain, phosphorylated domain.

Data deposition: The atomic coordinates reported in this paper have been deposited in the Protein Data Bank, www.rcsb.org (PDB ID code 1J97).

See commentary on page 8170.

‡To whom reprint requests should be addressed. E-mail: dewemmer@lbl.gov or kustu@nature.berkeley.edu.

¶Present address: Infectious Diseases Research, Lilly Research Laboratories, Indianapolis, IN 46285.

The publication costs of this article were defrayed in part by page charge payment. This article must therefore be hereby marked "*advertisement*" in accordance with 18 U.S.C. §1734 solely to indicate this fact.

the question of whether BeF_3^- might yield a persistent aspartyl phosphate analog in members of the HAD superfamily and thus facilitate structural studies of their conformations during catalysis.

We now report the structure of BeF_3^- complexed with PSP from the hyperthermophile *M. jannaschii*. NMR spectroscopy and biochemical studies indicated that BeF_3^- binds to the active site of PSP in solution and forms a tight persistent complex. Crystals of the complex, grown under conditions optimized by NMR spectroscopy, yielded a structure of BeF_3^-·PSP at 1.5-Å resolution. This allowed detailed definition of the active site and comparison of the overall structure and arrangement of active site residues to those in BeF_3^-·CheY.

Materials and Methods

Protein Samples and NMR. PSP from *M. jannaschii* was expressed and purified by using methods previously described (33). Uniformly ^{15}N-labeled samples of protein for NMR spectroscopy were prepared from cells grown in M9 minimal medium with [^{15}N]ammonium chloride as the sole nitrogen source. ^1H-^{15}N fast heteronuclear single quantum correlation (FHSQC) spectra were collected on an AMX 600 NMR spectrometer (Bruker Instruments, Billerica, MA).

Crystallization. PSP was concentrated to 54 mg/ml in a buffer containing 20 mM Tris·HCl, pH 7.5, 0.3 M NaCl, 1 mM EDTA, and 10 mM DTT. Crystals were grown by using the hanging drop vapor diffusion method with seeding. Concentrated NaF, $BeCl_2$, and $MgCl_2$ were added to the protein sample to final concentrations of 54 mM, 10.8 mM, and 90 mM, respectively. (CAUTION: Beryllium is toxic and immunogenic. Exercise care in its handling.) One microliter of this sample was then mixed with 1 μl of the reservoir well solution containing 0.1 M sodium acetate buffer at pH 4.5, 0.2 M sodium phosphate dihydrate, and 22% polyethylene glycol 2000 monomethylether (PEG2K MME). Microseeding was performed 1 h after the drop was set up. Crystals appeared within 12 h and reached a maximum size of $0.3 \times 0.5 \times 0.5$ mm. The concentration of PEG2K MME was then raised to 30% to stabilize the crystals.

Data Collection and Structure Refinement. A crystal from the crystallization drop was used directly for cryocrystallography data collection. X-ray diffraction data were collected at the Advanced Light Source (Lawrence Berkeley National Laboratory, Berkeley, CA) beam line 5.0.2 by using an Area Detector System Quantum 4 charge-coupled device detector placed 130 mm from the crystal. The data were processed by using the programs DENZO and SCALEPACK (34). X-ray data statistics are shown in Table 1.

The protein part of a previously determined PSP structure was used for initial rigid-body refinement to obtain a preliminary model (33). An electron density map calculated from this model clearly showed densities consistent with the fluorine atoms of a BeF_3^- that is bound to Asp-11 with a beryllium–oxygen bond distance of 1.55 Å. This density was used to build the beryllofluoride aspartate residue into the model that was further refined against data up to 1.5 Å by using the programs CNS (35) and O (36). The noncrystallographic symmetry constraints and restraints were completely released during the refinement. Ten percent of the data were randomly picked for free *R*-factor crossvalidation. The refinement statistics are shown in Table 1.

Phosphoserine Phosphatase Assay. The hydrolytic activity of PSP was measured at the desired temperature by the release of Pi from L-phosphoserine and is expressed as pmol Pi/min/pmol PSP. Assays were performed in triplicate in mixtures (50 μl) containing 20 mM Tris·Cl (pH 7.5), 1 mM $MgCl_2$, 5 mM L-phosphoserine, and different amounts of PSP. NaF (5 mM), $BeCl_2$ (100 μM), $AlCl_3$ (100 μM), or combinations were included in the mixture for inhibition assays. The reaction was stopped after 10 min by adding 5 μl of 0.2 M EDTA and placed on ice. The amount of inorganic phosphate released was determined with an EnzChek Phosphate Assay Kit (Molecular Probes).

Table 1. Summary of crystallographic analysis

Measurement	Value
Data collection	
Resolution limit, Å	1.5
Total reflections	288,900
Unique reflections	67,186
Completeness, %	93.8
R_{sym},* (%)	6.7
Refinement	
Resolution, Å	20–1.5
Number of protein atoms	3709
Number of water molecules	402
R_{cryst},† %	19.0
R_{free},‡ %	21.1
Average B, Å^2	14.77
rmsd bond length, Å	0.014
rmsd bond angles, degrees	1.80

rmsd, rms deviation.

*$R_{sym} = \Sigma_h\Sigma_i|I_{h,i} - \langle I\rangle_h|/\Sigma|\langle I\rangle_h|$, where I is the scaled intensity of the given reflection h.

†$R_{cryst} = \Sigma_h|F_{oh} - F_{ch}|/\Sigma_h F_{oh}$, where F_{oh}, and F_{ch} are the observed and calculated structure amplitudes for reflection h.

‡Value of R_{free} for 10% of randomly selected reflections excluded from the refinement.

Results

Inhibition of PSP Activity by BeF_3^- and Other Phosphate Analogues. Like phosphorylation, BeF_3^- activates various response regulators (10, 11). If BeF_3^- yielded an aspartyl phosphate analog in PSP, it would inhibit the activity of the enzyme by preventing substrate binding and/or formation of the phospho-PSP intermediate. At 50°C, the hydrolytic activity of PSP (100 nM) from *M. jannaschii* (840 ± 20 units) was markedly inhibited (>95%) in the presence of both $BeCl_2$ and NaF. The latter was provided at concentrations that yield predominantly $BeF3^-$ *in situ*. Either $BeCl_2$ or NaF alone had a much smaller inhibitory effect (35 or 20%, respectively). Similar inhibition by BeF_3^- was observed at room temperature or at 70°C (data not shown), the temperature at which the thermostable PSP from *M. jannaschii* showed maximum activity (33).

At 50°C, PSP activity (840 units, as above) was also inhibited in the presence of $AlCl_3$ and NaF (>85 vs. 30% in the presence of AlC_{l3} alone), which should generate predominantly AlF_3 and $AlF4^-$ *in situ* (37). Likewise, AlF_x yields an aspartyl phosphate analogue in response regulator CheY, activating it in a manner similar to phosphorylation or formation of a BeF_3^- complex (D.Y. and H.C., unpublished results). Orthovanadate, another phosphate analogue, inhibited the activity of *M. jannaschii* PSP (data not shown), as it did the activity of the human enzyme (21). The major difference among these phosphate analogs is the difference in their coordination geometries (37–39). Beryllofluoride yields a tetrahedral ground state analog of phosphate, whereas aluminum fluoride and vanadate often yield planar complexes that are analogues of phosphate during the transition state for transfer or hydrolysis.

Monitoring Formation of BeF_3^-·PSP Complexes by NMR Spectroscopy. Using ^1H-^{15}N FHSQC spectra, we could readily determine that BeF_3^- formed a persistent complex with PSP. As BeF_3^- was

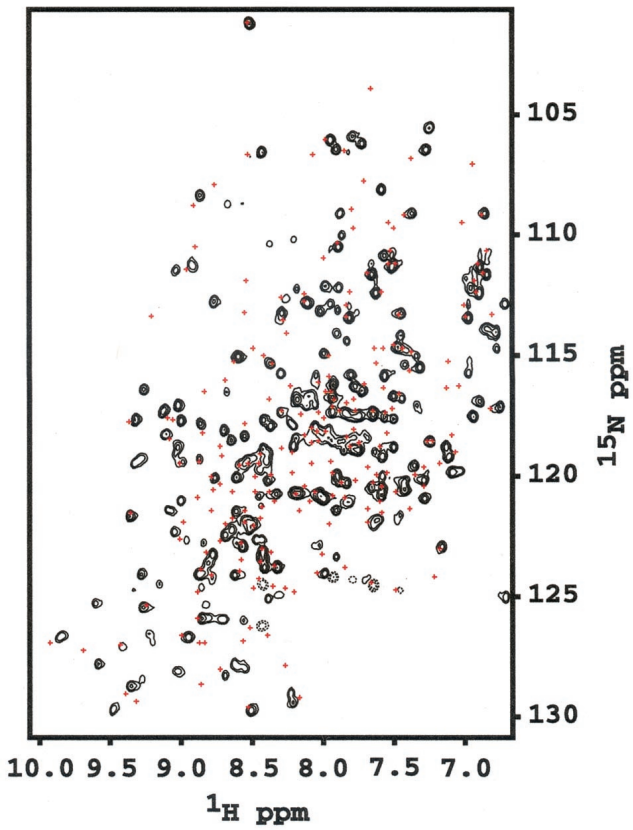

Fig. 1. ^{1}H-^{15}N FHSQC spectrum of BeF_3^-·PSP. PSP (0.5 mM) was incubated with 5 mM $MgCl_2$, 3 mM NaF, and 0.6 mM $BeCl_2$. Red crosses represent the crosspeak positions in the absence of NaF and $BeCl_2$. Spectra were recorded at 308 K and pH 6.5.

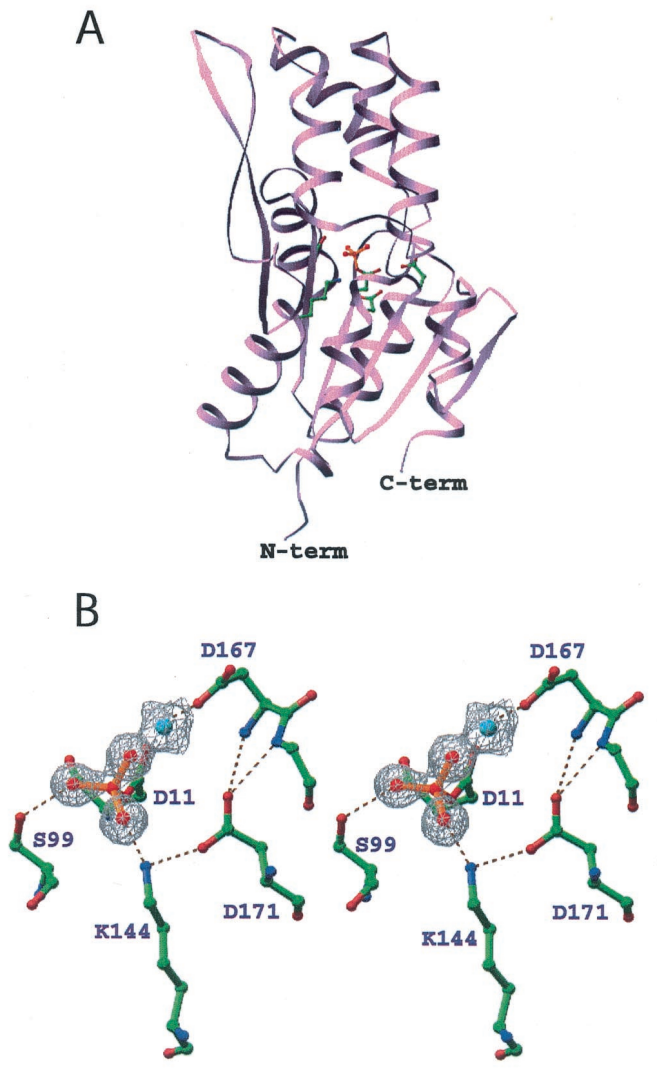

Fig. 2. Ribbon diagram of BeF_3^-·PSP (*A*) and stereoview of the active site (*B*). Ball-and-stick representations of the sidechain carbon, nitrogen, and oxygen atoms are colored green, blue, and red, respectively. In *A*, the sidechains of highly conserved active site residues, Asp-11, Ser-99, Lys-144, Asp-167, and Asp-171, are shown in ball-and-stick form. BeF_3^- (red balls and orange bonds) is bonded to Asp-11 Oδ in the center of the active site (33). In *B*, the $2F_o - F_c$ electron density map covering the magnesium (cyan) and fluorine (red) atoms was calculated in the absence of these atoms and is shown contoured at 1σ. The dashed lines represent hydrogen bonds, salt bridges, and metal–ligand interactions. Three of the Mg^{2+} ligands (two water molecules and Asp-13-C = O) are not shown.

added, many resonances doubled (Fig. 1). The lack of broadening of crosspeaks indicated that the dissociation rate of BeF_3^-·PSP complexes was slow (≤10 sec^{-1}). Surprisingly, addition of BeF_3^- to PSP changed the chemical shifts (crosspeak positions) of most of the backbone amides. By contrast, formation of BeF_3^- complexes of receiver domains changed the chemical shifts of the amides near the active site but of fewer farther away (10, 11); the latter effects occurred as a consequence of propagated conformational changes.

The FHSQC spectra provided a convenient means of optimizing conditions for quantitative conversion of PSP to BeF_3^-·PSP complexes. Unfortunately, PSP could not be maintained in a phosphorylated state long enough to collect data for the phosphoenzyme intermediate (data not shown).

Crystal Structure of BeF_3^-·PSP. In the crystal structure of BeF_3^-·PSP (Fig. 2*A*), the active site in the core α/β domain is covered by the four-helix bundle domain. BeF_3^- is bound to Asp-11 in the α/β domain, which is the site of phosphorylation (14) and is surrounded by the sidechains of residues that are highly conserved in the HAD superfamily of proteins. The overall protein structure is very similar to a recently solved structure of PSP containing a phosphate (PO_4^{2-}) in the active site (33).

Active Site of BeF_3^-·PSP. In *M. jannaschii* PSP, the quintet of conserved residues found in HAD family members that form a phosphoaspartate intermediate are: Asp-11, the site of phosphorylation, Ser-99, Lys-144, Asp-167, and Asp-171. With the exception of Ser-99 to Thr, mutational change of any of the corresponding residues in human PSP dramatically decreased catalytic efficiency (40). These conserved residues come together in the active site to bind BeF_3^- and the essential divalent cation Mg^{2+} (Fig. 2*B*). The Asp 11-Oδ1 is bound to beryllium with an O-Be distance of 1.5 Å. Asp-11-Oδ2, along with a fluorine, Asp-13-C = O, Asp-167-Oδ, and two water molecules occupy the six coordination sites of Mg^{2+}. Ser-99-Oγ forms a hydrogen bond with BeF_3^-. Lys-144-Nζ forms salt bridges with BeF_3^- and Asp-171-Oδ1. Asp-171-Oδ2 forms hydrogen bonds with the backbone amides of Asp-167 and Gly-168. These two hydrogen bonds appear to stabilize the conformation of the backbone around Asp-167 such that the Asp-167 sidechain is restrained to a position that allows it to coordinate Mg^{2+} (see *Discussion*).

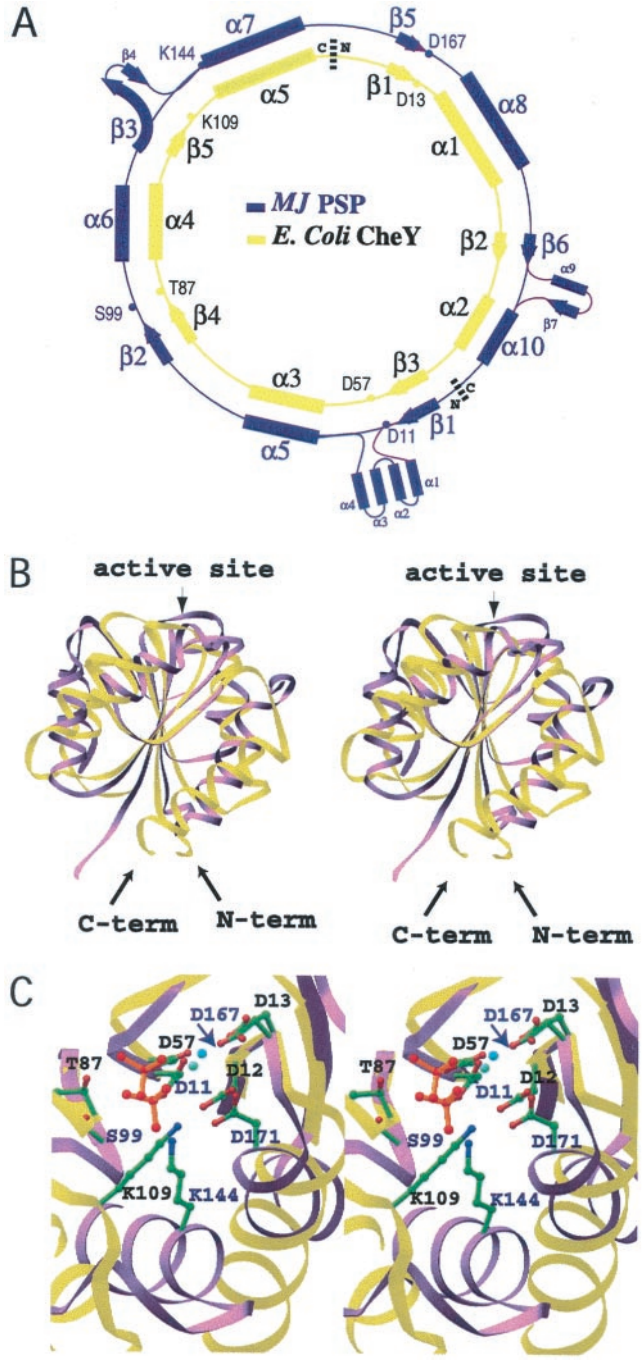

Fig. 3. Alignment and stereoviews showing the superposition of BeF_3^-·PSP and BeF_3^-·CheY. Structurally homologous β-strand residues (PSP: 7–11, 94–98, 116–120, 162–167, 180–182, and CheY: 53–57, 82–86, 104–108, 8–13, 34–36) were used for the superposition. PSP and CheY are colored purple and yellow, respectively. (*A*) Diagram of the circular permutation required to align the conserved active site residues of PSP and CheY (29). (*B*) Ribbon structures of PSP and CheY. The molecules are oriented with the H4-β5-H5 face of CheY directed toward the reader. The N and C termini of CheY are denoted. Some PSP residues that have no structural counterparts in CheY are not shown. (*C*) A top-down view of the superimposed active sites. This orientation was obtained by applying a $-90°$ rotation around the *x*-axis starting from the orientation in *B*. The active site residues of PSP and CheY are labeled in purple and black, respectively. The sidechains are shown in ball-and-stick form with carbon, nitrogen, and oxygen atoms colored green, blue, and red, respectively. BeF_3^- is represented by red balls with orange bonds. The cyan- and blue-green-colored balls, lower and upper, respectively, adjacent to BeF_3^- represent the Mg^{2+} ions in the PSP and CheY structures, respectively. The purple arrow points to D167 of PSP.

Discussion

Comparison of BeF_3^-·PSP and BeF_3^-·CheY: The "Stabilized Mg^{2+} Chelation Loop." Despite the circular permutation required to align their primary sequences (29) (Fig. 3*A*), superposition of the structurally homologous β-strand residues of BeF_3^-·PSP and BeF_3^-·CheY (41) results in an rms deviation of only 0.6 Å and shows that the core β-sheets have a similar curvature (Fig. 3*B*). By contrast, the α-helices in the α/β domains of the two proteins show large differences in position. Comparison of their active sites reveals that the conserved quintet of residues in PSP and CheY chelate BeF_3^- and Mg^{2+} similarly and form very similar hydrogen bonds and salt bridges (Fig. 3*C*). PSP residues Asp-11, Ser-99, and Asp-167, whose roles are discussed in *Results*, are functionally and structurally equivalent to CheY residues Asp-57, Thr-87, and Asp-13, respectively. PSP residues Lys-144 and Asp-171 appear to be functionally equivalent to CheY residues Lys-109 and Asp-12, respectively, although these residues originate from different secondary structural elements. Lys-144 (PSP) originates from an α-helix, whereas Lys-109 (CheY) originates from a loop; likewise, Asp-171 (PSP) originates from an α-helix, whereas Asp-12 (CheY) originates from the C terminus of a β-strand. Despite the differences in their position of origin, the amino groups of Lys-144 (PSP) and Lys-109 (CheY) reach comparable positions in the active site and form salt bridges with BeF_3^- and an aspartate residue, Asp-171 (PSP) and Asp-12 (CheY).

The pairs of functionally analogous aspartate residues Asp-167 and Asp-171 of PSP and Asp-13 and Asp-12 of CheY play surprisingly similar roles in Mg^{2+} coordination (Figs. 2*B* and 3*C*), despite the fact that they are inverted with respect to one another and separated by different numbers of residues. In PSP, the first residue of the pair in the primary sequence, Asp-167, acts as a direct ligand to Mg^{2+}, whereas in CheY it is the second, Asp-13. Asp-167 (PSP) and Asp-13 (CheY) are located in similar loops that are stabilized by main chain hydrogen bonds to the other aspartates of the respective pairs, Asp-171 (PSP) and Asp-12 (CheY) ("stabilized Mg^{2+} chelation loops"). The stabilizing aspartates also form salt bridges to the highly conserved lysine residues, Lys-144 (PSP) and Lys-109 (CheY) and hence are precisely positioned. Remarkably, the aspartate that functions as a direct Mg^{2+} ligand is not conserved in HAD family proteins that do not require a divalent cation for activity (12, 13).

Hypotheses Regarding the Function of PSP and the Ca^{2+}-ATPase. The two domains of PSP appear to be in a "closed configuration" in the BeF_3^-·PSP complex (Fig. 2*A*) (33): the helical domain, which presumably participates in binding the substrate phosphoserine, completely shields the active site of the α/β domain from solvent. In this closed configuration of PSP, it would be impossible for substrate to enter or product to be released. It is likely that the widespread changes in the ^1H-^{15}N FHSQC spectrum of PSP on addition of BeF_3^- (Fig. 1) are at least partially caused by a transition of its two domains from a more open to this closed configuration. Such a transition might contribute to a high degree of specificity of the enzyme for phosphoserine (21), a necessity for the function of an intracytoplasmic phosphatase, and/or to the poor reversibility of phosphoserine hydrolysis. The closed configuration of BeF_3^-·PSP presumably mimics one from which phosphate would be hydrolyzed (33).

Although the Ca^{2+}-ATPase of rabbit sarcoplasmic reticulum has a much more complicated domain structure than PSP or CheY (32) (Fig. 4*A*), there are nonetheless striking parallels among these three proteins. The phosphorylated (P) domain of the Ca^{2+}-ATPase is structurally homologous to the core α/β domain of PSP and to CheY. Asp-703 in the P domain lies in a stabilized Mg^{2+} chelation loop similar to those of PSP and

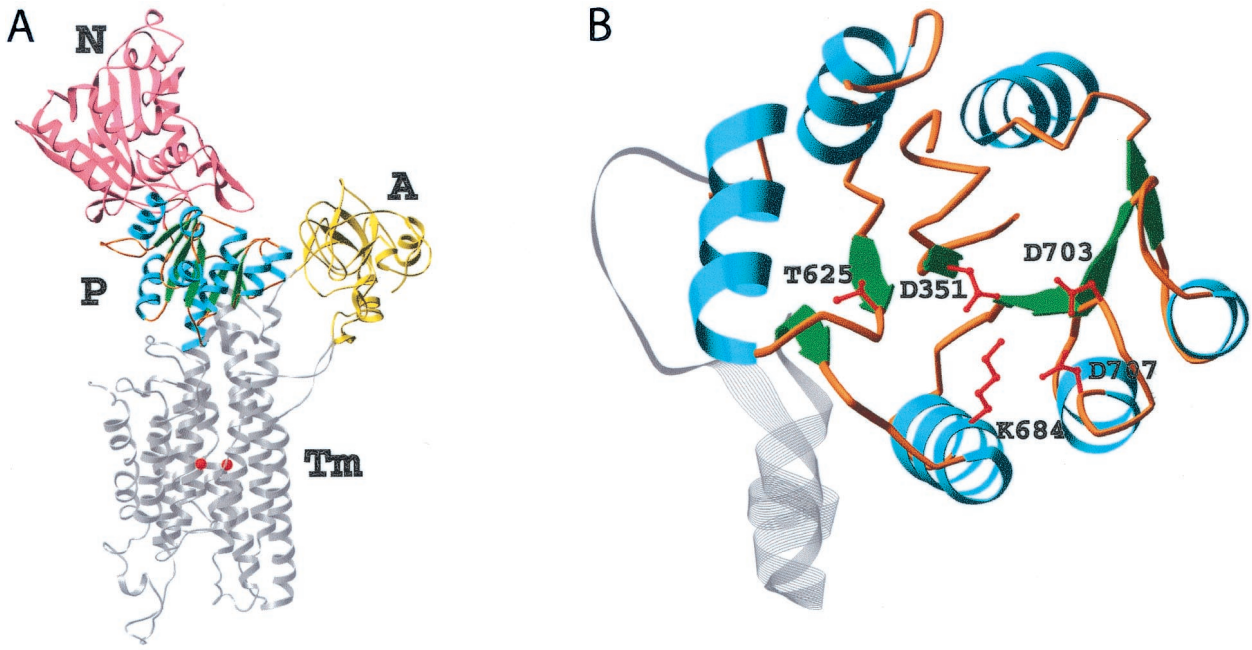

Fig. 4. Ribbon diagrams of the Ca^{2+}-ATPase from rabbit sarcoplasmic reticulum (*A*) and its catalytic P domain (*B*) [drawn from coordinates of Toyoshima *et al.* (32)]. (*A*) The N (nucleotide-binding), A (actuator), and M (Ca^{2+}-binding) domains are shown in pink, yellow, and gray, respectively. The latter traverses the membrane of the sarcoplasmic reticulum. The two Ca^{2+} ions are shown in red. The catalytic P domain is shown in blue (helices), green (β-strands), and orange (loops). (*B*) This top-down view was obtained by applying a $-90°$ rotation around the *x*-axis starting from the orientation in *A*. The quintet of conserved residues in the P domain is shown in ball-and-stick form in red. Mg^{2+} was apparently not present in this domain.

CheY. Asp-703 is correctly positioned to coordinate Mg^{2+} by means of hydrogen bonds between this loop and the stabilizing aspartate Asp-707. Conceptually, the nucleotide-binding (N) domain of the Ca^{2+}-ATPase, which binds ATP and delivers its γ phosphate to the active-site aspartate in the P domain, has a role related to that of the helical domain of PSP or that of CheA, the cognate histidine autokinase for CheY. The small actuator domain of the ATPase, its third cytoplasmic domain, is unique.

As is the case for CheY and other receiver domains, the P domain of the intact Ca^{2+}-ATPase can be phosphorylated by acetylphosphate rather than ATP (16, 17, 42), an activity that presumably does not depend on its N domain. Phosphorylation by either donor acts as a key switch during Ca^{2+} transport (16, 17, 42). Formation of the first phosphoenzyme intermediate, $E_1MgP\cdot(Ca^{2+})_2$, results in occlusion of calcium within the membrane-spanning portion of the protein. In a conformational change(s) that is a rate-limiting step in the catalytic cycle, this intermediate then yields E_2MgP as a consequence of diffusion of the occluded calcium to lower affinity sites and its release into the lumen of the sarcoplasmic reticulum. Finally, the enzyme is regenerated by dephosphorylation. Because the site of phosphorylation in the Ca^{2+}-ATPase is more than 50 Å away from the Ca^{2+}-binding sites (32), formation of the phosphoaspartate bond must be coupled to a conformational change(s) within the P domain that is propagated to the transmembrane, Ca^{2+}-binding domain. Given the comparable interactions in the active sites of $BeF_3^-\cdot$PSP and $BeF_3^-\cdot$CheY (Fig. 3*C*), the phosphorylation-induced conformational change within the P domain of the Ca^{2+}-ATPase is likely to be driven by a mechanism similar to that used in receiver domains. In CheY, this mechanism appears to entail the formation of a hydrogen bond between the hydroxyl group of Thr-87 and aspartyl phosphate (or BeF_3^-) and the replacement of a salt bridge between the amino group of Lys-109 and the carboxyl group of the active site aspartate by one to the modified aspartate (6, 7, 10, 43). Analogies between interactions in the active sites of $BeF_3^-\cdot$PSP and activated CheY (Fig. 3*C*) provide evidence that Thr-625 and Lys-684, respectively, of the Ca^{2+}-ATPase form the corresponding hydrogen bond and salt bridge to the phosphoaspartate, as previously postulated (29). In the structure of the unphosphorylated calcium-bound form of the ATPase that has been determined (32), Lys-684 appears to form a salt bridge to Asp-351 that is similar to the salt bridge between Lys-109 and Asp-57 in inactive CheY (44). However, the sidechains of Thr-625 and Asp-351 are separated by 7.4 Å, a distance that cannot be bridged by a hydrogen bond and a phosphoryl group without a conformational change. As in receiver domains, the movement of the sidechains of Thr-625 and Lys-684 on phosphorylation of Asp-351 might stabilize a conformational change within the P domain of the Ca^{2+}-ATPase that is propagated into the downstream transmembrane domain. Given that $E_1MgP\cdot(Ca^{2+})_2$ and E_2MgP are likely to be extremely difficult to trap for structural work, these hypothetical sidechain movements and the accompanying more extensive conformational changes might best be evaluated by crystallization of the corresponding BeF_3^- complexes. These would be structurally equivalent to the phosphorylated complexes but persistent.

Use of BeF_3^- as a Phosphate Analogue. Originally, BeF_3^- was used in biochemical and structural studies of G proteins and later of myosin, the F1-ATPase, nitrogenase, and some kinases (38, 39, 45). In these earlier cases, high-affinity binding of BeF_3^- required the presence of a purine nucleoside diphosphate (GDP or ADP) in the nucleotide-binding site of the enzyme, and BeF_3^- served as an analogue of the γ-phosphate in its ground state. Recently, BeF_3^- has been used to generate an analogue of aspartyl phosphate in response regulators, providing a convenient and apparently general means of mimicking their active phosphorylated forms (11). As discussed in this work, we have now extended the use of BeF_3^- to structural studies of members of the

HAD superfamily. The BeF_3^-·PSP complex mimics a phosphoenzyme intermediate for this enzyme (half-life ≤ 0.1 sec at 50°C), which was so labile that the phosphorylation of aspartate could not be confirmed chemically (14). Biochemical studies indicate that BeF_3^- forms an aspartyl phosphate mimic in the Ca^{2+}-ATPase from rabbit sarcoplasmic reticulum (24). The stable BeF_3^--ATPase complex is rapidly disrupted by luminal Ca^{2+} (24), and hence it appears to resemble most closely E_2MgP. Structural analogies between PSP, CheY, and the Ca^{2+}-ATPase make it likely that BeF_3^- complexes will be useful in defining the conformational changes that allow P-type ATPases to couple the energy available from ATP hydrolysis to transport of cations (15–17, 32).

We thank our colleagues B. T. Nixon for critical review of the manuscript and Ore Carmi for help in its preparation. This work was supported by U.S. Department of Energy Contract No. DE-AC03–76SF0098 to D.W., S.-H.K., and R.K., National Institutes of Health (NIH) Grant P50 GM62412 to S.-H.K. and R.K., NIH Grant GM62163 to D.W., and NIH Grant GM38361 to S.K.

1. Post, R. L. & Kume, S. (1973) *J. Biol. Chem.* **248,** 6993–7000.
2. Weiss, V. & Magasanik, B. (1988) *Proc. Natl. Acad. Sci. USA* **85,** 8919–8923.
3. Hoch, J. A. & Silhavy, T. J. (1995) *Two-Component Signal Transduction* (Am. Soc. Microbiol., Washington, DC).
4. Djordjevic, S. & Stock, A. M. (1998) *J. Struct. Biol.* **124,** 189–200.
5. Falke, J. J., Bass, R. B., Butler, S. L., Chervitz, S. A. & Danielson, M. A. (1997) *Annu. Rev. Cell Dev. Biol.* **13,** 457–512.
6. Birck, C., Mourey, L., Gouet, P., Fabry, B., Schumacher, J., Rousseau, P., Kahn, D. & Samama, J. P. (1999) *Struct. Folding Des.* **7,** 1505–1515.
7. Lewis, R. J., Brannigan, J. A., Muchová, K., Barák, I. & Wilkinson, A. J. (1999) *J. Mol. Biol.* **294,** 9–15.
8. Kern, D., Volkman, B. F., Luginbühl, P., Nohaile, M. J., Kustu, S. & Wemmer, D. E. (1999) *Nature (London)* **402,** 894–898.
9. Halkides, C. J., McEvoy, M. M., Casper, E., Matsumura, P., Volz, K. & Dahlquist, F. W. (2000) *Biochemistry* **39,** 5280–5286.
10. Cho, H. S., Lee, S. Y., Yan, D., Pan, X., Parkinson, J. S., Kustu, S., Wemmer, D. E. & Pelton, J. G. (2000) *J. Mol. Biol.* **297,** 543–551.
11. Yan, D., Cho, H. S., Hastings, C. A., Igo, M. M., Lee, S. Y., Pelton, J. G., Stewart, V., Wemmer, D. E. & Kustu, S. (1999) *Proc. Natl. Acad. Sci. USA* **96,** 14789–14794.
12. Aravind, L., Galperin, M. Y. & Koonin, E. V. (1998) *Trends Biochem. Sci.* **23,** 127–129.
13. Koonin, E. V. & Tatusov, R. L. (1994) *J. Mol. Biol.* **244,** 125–132.
14. Collet, J. F., Stroobant, V., Pirard, M., Delpierre, G. & Van Schaftingen, E. (1998) *J. Biol. Chem.* **273,** 14107–14112.
15. Jencks, W. P. (1995) *Biosci. Rep.* **15,** 283–287.
16. McIntosh, D. B. (2000) *Nat. Struct. Biol.* **7,** 532–535.
17. MacLennan, D. H. & Green, N. M. (2000) *Nature (London)* **405,** 633–634.
18. Seal, S. N. & Rose, Z. B. (1987) *J. Biol. Chem.* **262,** 13496–13500.
19. Pirard, M., Collet, J. F., Matthijs, G. & Van Schaftingen, E. (1997) *FEBS Lett.* **411,** 251–254.
20. Collet, J. F., Gerin, I., Rider, M. H., Veiga-da-Cunha, M. & Van Schaftingen, E. (1997) *FEBS Lett.* **408,** 281–284.
21. Veeranna & Shetty, K. T. (1990) *Neurochem. Res.* **15,** 1203–1210.
22. Cantley, L. C., Jr., Cantley, L. G. & Josephson, L. (1978) *J. Biol. Chem.* **253,** 7361–7368.
23. Missiaen, L., Wuytack, F., De Smedt, H., Vrolix, M. & Casteels, R. (1988) *Biochem. J.* **253,** 827–833.
24. Murphy, A. J. & Coll, R. J. (1993) *J. Biol. Chem.* **268,** 23307–23310.
25. Pick, U. (1982) *J. Biol. Chem.* **257,** 6111–6119.
26. Rapin-Legroux, C., Troullier, A., Dufour, J.-P. & Dupont, Y. (1994) *Biochim. Biophys. Acta* **1184,** 127–133.
27. Robinson, J. D., Davis, R. L. & Steinberg, M. (1986) *J. Bioenerg. Biomembr.* **18,** 521–531.
28. Troullier, A., Girardet, J. L. & Dupont, Y. (1992) *J. Biol. Chem.* **267,** 22821–22829.
29. Ridder, I. S. & Dijkstra, B. W. (1999) *Biochem. J.* **339,** 223–226.
30. Hisano, T., Hata, Y., Fujii, T., Liu, J. Q., Kurihara, T., Esaki, N. & Soda, K. (1996) *J. Biol. Chem.* **271,** 20322–20330.
31. Ridder, I. S., Rozeboom, H. J., Kalk, K. H., Janssen, D. B. & Dijkstra, B. W. (1997) *J. Biol. Chem.* **272,** 33015–33022.
32. Toyoshima, C., Nakasako, M., Nomura, H. & Ogawa, H. (2000) *Nature (London)* **405,** 647–655.
33. Wang, W., Kim, R., Jancarik, J., Yokota, H. & Kim, S. H. (2001) *Struct. Folding Des.* **9,** 65–72.
34. Otwinowski, Z. & Minor, W. (1996) *Methods Enzymol.* **276,** 307–326.
35. Brünger, A. T., Adams, P. D., Clore, G. M., DeLano, W. L., Gros, P., Grosse-Kunstleve, R. W., Jiang, J. S., Kuszewski, J., Nilges, M., Pannu, N. S., *et al.* (1998) *Acta Crystallogr. D* **54,** 905–921.
36. Jones, T. A., Zou, J. Y., Cowan, S. W. & Kjeldgaard. (1991) *Acta Crystallogr.* **47,** 110–119.
37. Martin, R. B. (1988) *Biochem. Biophys. Res. Commun.* **155,** 1194–1200.
38. Chabre, M. (1990) *Trends Biochem. Sci.* **15,** 6–10.
39. Petsko, G. A. (2000) *Proc. Natl. Acad. Sci. USA* **97,** 538–540.
40. Collet, J. F., Stroobant, V. & Van Schaftingen, E. (1999) *J. Biol. Chem.* **274,** 33985–33990.
41. Lee, S. Y., Cho, H. S., Pelton, J. G., Yan, D., Henderson, R. K., King, D. S., Huang, L. S., Kustu, S., Berry, E. A. & Wemmer, D. E. (2001) *Nat. Struct. Biol.* **8,** 52–56.
42. Bodley, A. L. & Jencks, W. P. (1987) *J. Biol. Chem.* **262,** 13997–14004.
43. Lee, S.-Y., Cho, H. S., Pelton, J. G., Yan, D., Berry, E. & Wemmer, D. E. (2001) *J. Biol. Chem.* **276,** 16425–16431.
44. Stock, A. M., Mottonen, J. M., Stock, J. B. & Schutt, C. E. (1989) *Nature (London)* **337,** 745–749.
45. Xu, Y. W., Moréra, S., Janin, J. & Cherfils, J. (1997) *Proc. Natl. Acad. Sci. USA* **94,** 3579–3583.